Polar vortex strength impacts on the longitudinal structure of thermospheric composition and ionospheric electron density

K. R. Greer[1], L. P. Goncharenko[2,3], V. L. Harvey[1], and N. Pedatella[4]

[1] Laboratory for Atmospheric and Space Physics, University of Colorado, Boulder, CO, USA
[2] Haystack Observatory, Massachusetts Institute of Technology, Westford, Massachusetts, USA
[3] Leibniz Institute of Atmospheric Physics at the University of Rostock, Germany
[4] High Altitude Observatory, National Center for Atmospheric Research, Boulder, CO, USA
Corresponding author: Katelynn R. Greer (katelynn.greer@lasp.colorado.edu)

Key Points:

- For the first time, a strong polar vortex event is shown to have an impact on both ionospheric electron density and O/N_2 at midlatitudes.
- Both strong and weak vortex events have an influence on thermospheric composition, presumably through modified thermospheric circulation.
- Regions of enhanced O/N_2 coincide with elevated Total Electron Content in the Asian sector during the strong vortex event.

Abstract

This work examines the weak stratospheric polar vortex (SPV) event of February 2008 and the strong SPV event of February 2021 to understand the potential influence of SPV strength on midlatitude thermospheric composition and ionospheric plasma density. The weak SPV event shows a reduction in thermospheric O/N_2 at all longitudes, changes in the ionospheric total electron content (TEC) that vary with longitude, and an intensification of the semidiurnal tides. The strong SPV event shows O/N_2 elevated by up to 25% in the Asian sector and a 25% decrease in semidiurnal tidal amplitude. The TEC response during the strong SPV event is complex, but shows enhanced TEC in the Asian sector where O/N_2 is elevated. These are the first observations of anomalies in the thermospheric composition and ionospheric plasma associated with a strong polar vortex event.

Plain Language Summary

The stratospheric polar vortex is a belt of westerly winds in the midlatitudes that exists in the middle atmosphere during the winter months. However, the polar vortex is highly variable; sometimes it is weak and distorted while other times it is strong. Vortex strength is known to impact weather in the troposphere and variability in the mesosphere, thermosphere, and ionosphere. The state of the polar vortex is predictable up to two weeks in advance, so knowledge of the vortex may increase predictability in other regions of the atmosphere. Here we use two case studies to examine how a weak vortex and a strong vortex impact the composition of the thermosphere and the density of the ionosphere at midlatitudes. During the weak vortex case, the thermospheric composition is changed such that there is a decrease in the ratio of atomic oxygen to molecular nitrogen (O/N_2). However, during the strong vortex case, there are longitude sectors that see elevated values of O/N_2. These regions of elevated O/N_2 correspond to increased ionospheric plasma density. These are the first observations of anomalies in the thermosphere and ionosphere associated with a strong vortex event.

1. Introduction

In the polar winter stratosphere and mesosphere, the most notable dynamical feature is the polar vortex (e.g., Schoeberl et al., 1992; Harvey et al., 2018) which is characterized by a belt of intense westerly winds in midlatitudes that encircle cold air over the pole (see Harvey et al., 2002 and references therein). It is well known that the polar vortex acts to couple surface weather to space weather through the generation and modulation of gravity waves, as well as the modulation of tides and planetary waves (e.g., Chau et al., 2009; Kuroda and Kodera, 1999; Miyoshi et al., 2015; Oberheide et al., 2020, Pedatella et al., 2012). Of particular interest here is the impact of polar vortex strength on thermospheric and ionospheric variability (see Harvey et al., 2022).

The Arctic polar vortex is highly variable in strength, shape, and position (Lawrence and Manney, 2018). For example, the Arctic polar vortex often weakens as a result of upward propagating planetary waves (PWs) which can lead to Sudden Stratospheric Warmings (SSWs) (Scherhag, 1952; Limpasuvan et al., 2004; Matsuno, 1971). SSWs are characterized by warming of the polar stratosphere by tens of degrees in several days and dramatic weakening or even reversal of the zonal mean zonal winds (e.g., Charlton & Polvani, 2007). Associated with SSWs is an increase in the amplitude of semidiurnal solar and the lunar tides (Chau et al., 2015;

Goncharenko et al., 2012; Limpasuvan et al., 2016; McDonald et al., 2018; Pedatella et al., 2012; Sathiskumar and Sridharan, 2013; Zhang and Forbes, 2014), which can influence the thermosphere and ionosphere through multiple mechanisms, including modification of electric fields (Fejer et al., 2010; Jin et al., 2012), upper thermospheric winds (Pedatella and Maute, 2015), and thermospheric composition caused by tidal dissipation (Jones et al., 2014b; Oberheide et al., 2020; Yamazaki & Richmond, 2013).

Many studies have focused on the impacts of a weak polar vortex (i.e., SSWs) on the troposphere below (Baldwin et al., 2021) and the ionosphere above (Chau et al., 2012; Goncharenko et al., 2021a). Reviews by Chau et al. (2012) and Goncharenko et al. (2021b) summarize the changes in thermospheric composition, temperature, and winds as well as changes in ionospheric plasma densities and electrodynamics during weak polar vortex states. However, there have been relatively few studies of strong polar vortex events and their effects on the thermosphere and ionosphere. Pedatella and Harvey (2022) examined the zonal mean temperature, circulation, and atmospheric tides in the mesosphere and lower thermosphere and found that simulated strong polar vortex events were associated with a *decrease* in the migrating semidiurnal solar tide (SW2) amplitudes by 25-35% compared to climatology. Pedatella (2023) used model ensembles to examine the average change in zonal mean thermospheric composition and ionospheric density, finding decreases of 1-2% and 5-10%, respectively. This work provides the first observations of anomalous thermosphere composition and ionosphere density during strong vortex events using satellite and ground-based observations. Results demonstrate opposite anomalies in the thermosphere-ionosphere occur during weak and strong vortex events.

2. Observations, Models, and Methods

Aura Microwave Limb Sounder (MLS) satellite observations (Waters et al., 2006) are used to establish middle atmospheric dynamical conditions during the weak and strong vortex case studies. MLS version 5.1 temperatures, carbon monoxide (CO), and zonal winds derived from geopotential height are utilized. The temperature and geopotential height data products are similar to previous versions described in Schwartz et al. (2008). The geopotential height observations are used to derive daily mean geostrophic winds. Daily zonal means are calculated at each pressure level in 1.9° latitude bins by combining both the daytime (13:30 LT) and nighttime observations (1:30 LT) to reduce tidal effects.

Simulations of the Specified Dynamics version of the Whole Atmosphere Community Climate Model with thermosphere-ionosphere eXtension (SD-WACCM-X) are used to further examine conditions in the middle and upper atmosphere during these events. WACCM-X is a whole atmosphere model that extends from the surface to the upper thermosphere (Liu et al., 2018). The SD version reproduces observed atmospheric variability by constraining model meteorology up to ~50 km using the Modern-Era Retrospective analysis for Research and Applications version 2 (MERRA-2) (Gelaro et al., 2017; Smith et al., 2017). For more information on these model runs, see Pedatella & Harvey (2022). Similar to Pedatella & Harvey (2022), we calculate anomalies relative to the 1980-2017 model climatology.

The O/N_2 data used is from the Thermosphere, Ionosphere, Mesosphere, Energetics, and Dynamics (TIMED) Global UltraViolet Imager (GUVI) instrument (Meier et al., 2015), version

13. The GUVI instrument provides O/N_2 on Earth's day side. The GUVI disk dayglow data at O (135.6 nm) and N2 LBH (140–150 nm) have been used to derive $\sum O/N_2$ referenced at a fixed N_2 column density of $1x10^{17}$ cm^{-2}, here referred to as simply O/N_2.

To examine ionospheric variations, we used Total Electron Content (TEC) data provided by the CEDAR Madrigal database and processed at the MIT Haystack Observatory (Rideout and Coster, 2006; Vierinen et al., 2016). The TEC data is based on observations of line-of-sight TEC between ~6000 ground-based receivers and satellite navigation systems. We used a TEC data product that has 1 × 1 degree latitude by longitude resolution every 5 minutes, and provides excellent coverage over the continental U.S., Europe, and parts of Asia.

3. Results & Discussion

3.1 Middle Atmosphere Conditions During the Weak & Strong Vortex Case Studies

Figure 1 illustrates the middle atmosphere dynamical conditions during the two selected case studies: the weak vortex event of 26 February 2008 (left column) and the strong vortex event of 26 February 2021 (right column). These particular events were chosen for their data availability, low solar flux conditions, low geomagnetic activity, and same seasonality. These events further satisfy the Northern Annular Mode (NAM) index criteria used by Pedatella & Harvey (2022). In the top row (panels a and b), the filled colors are the MLS zonal mean temperature anomalies (deviations from the time mean), the solid and dashed black lines are zonal mean zonal winds, and the thick red contour is the 0.5 ppmv CO isoline, a proxy for descent. In the weak vortex case (panel a) the following is observed: (1) alternating warm, cold, warm temperature anomalies in the polar stratosphere, lower mesosphere, and upper mesosphere, respectively (Randel, 1993; Limpasuvan et al., 2016), (2) easterly winds at 70°N and 30 km and a weak (~45 m/s) polar night jet max near 50°N and 50 km, and (3) weak polar descent as evidenced by a relatively flat CO contour. In the strong vortex case (panel b) the opposite occurs: (1) alternating cold, warm, cold temperature anomalies in the polar stratosphere, lower mesosphere, and upper mesosphere, respectively, (2) ~45 m/s westerly winds at 70°N and 30 km and a strong (>90 m/s) polar night jet max near 50°N and 50 km, and (3) strong polar descent as deduced from the CO contour that is displaced downward at high latitudes. The remaining panels of the figure are from SD-WACCM-X simulations of the events. The simulated zonal mean zonal winds and temperature anomalies (panels c and d) are generally consistent with the observations, confirming that the model accurately represents the events. In panels (e) and (f), the change in the SW2 amplitude is shown. During the weak vortex event (panel e), there is an increase in the SW2 amplitude of 10 m/s (~30%) at midlatitudes in the lower thermosphere; this agrees with previous studies (e.g., Goncharenko et al., 2021b). The strong vortex event (panel f) shows an opposite behavior with a decrease in the SW2 amplitude of 8 m/s (~25%). Panels (g-j) show the residual circulation anomalies (in color) and the residual circulation vectors (black arrows). The large gray arrows indicate the general direction of the residual circulation. In the weak vortex case (panels g and i), there is Equator to pole flow between 110-140 km, with descent at these altitudes over the pole, but ascent below (consistent with the CO isoline from panel a), consistent with Miyoshi et al., (2015). In contrast, during the strong vortex event (panels h and j), there is descent above 140 km over the pole and a pole to Equator flow between 110-140 km.

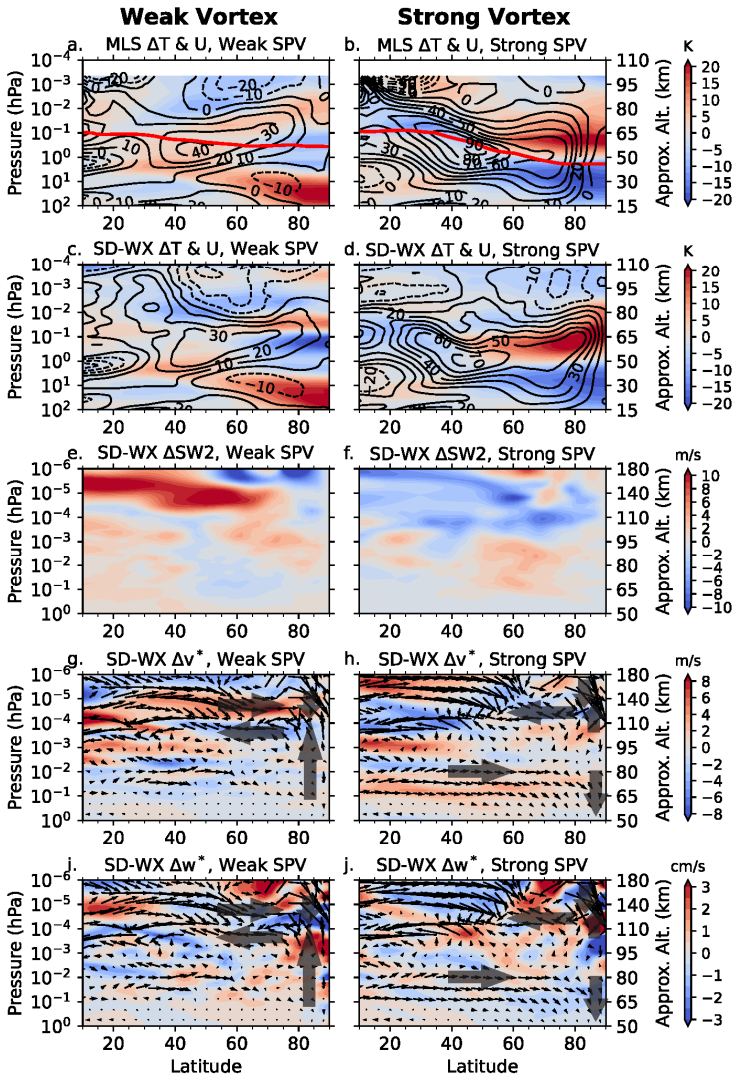

Figure 1. MLS temperature deviation from the 2005-2022 mean on February 26 (in color), zonal mean zonal winds (black lines), and the 0.5 CO ppmv isoline (red line) for a weak vortex (panel a) and a strong vortex (panel b). Panels (c) and (d) are the same as (a) and (b) but for SD-WACCM-X. Panels (e) and (f) show anomalies in the SW2. Panels (g)-(j) show the change in residual circulation (in color), the residual circulation (black vectors), and general circulation (transparent gray arrows).

3.2 Baseline Conditions

For this study we computed baseline conditions (climatology) for both thermospheric O/N_2 and ionospheric TEC. The purpose of these climatologies is to quantify anomalies caused by weak or strong polar vortices and account for impacts of solar and geomagnetic activity.

Climatological medians of O/N_2 were computed using the following requirements: (a) observations collected between 2008-2022, (b) F10.7 solar flux between 65 and 80 sfu, (c) geomagnetic index ap less than 13 for the day in question as well as the previous day, and (d) non-major SSW conditions. The bins are +/- 10 days around the central date, +/- 7.5° longitude, +/- 2.5° latitude, and +/- 45 minutes. Figure 2 shows O/N_2 (panels a and c) and TEC (panels b and d) climatologies at 15 local time (LT) (top panels) and 10 LT (bottom panels) on 26 February. These LTs were selected based on available GUVI observations during the two events. It is important to note that at a fixed geographic latitude a significant portion of the longitudinal variability of O/N_2 at a given LT is due to variations in geomagnetic latitude (Qian et al., 2016). For that reason, we include a reference of 35° magnetic latitude (white contour). This magnetic latitude was selected to avoid contamination by the Equatorial Ionization Anomaly (EIA) and the auroral oval. All further data analysis will be performed at this geomagnetic latitude to limit the influence of the configuration of Earth's geomagnetic field on the O/N_2 results. In these climatologies, it is evident that there is a strong LT variation in O/N_2 and O/N_2 is higher in the morning hours of the 26 February climatology than the afternoon hours. We note that this LT behavior is consistent with observations by Global-scale Observations of Limb and Disk (Gan et al., 2023) and could be driven by atmospheric tides.

Figure 2, panels (b) and (d) show the TEC climatologies. The median TEC values were calculated for the same dates as in the O/N_2 climatology, but TEC data has a 1x1 degree resolution in longitude and latitude, as well as 30-minute temporal resolution. Further descriptions of the development of the baseline TEC can be found in Goncharenko et al. (2020). Figures 2b and 2d show a clear longitudinal and latitudinal variability of TEC, which is influenced by several factors including composition, neutral dynamics, and the electric field.

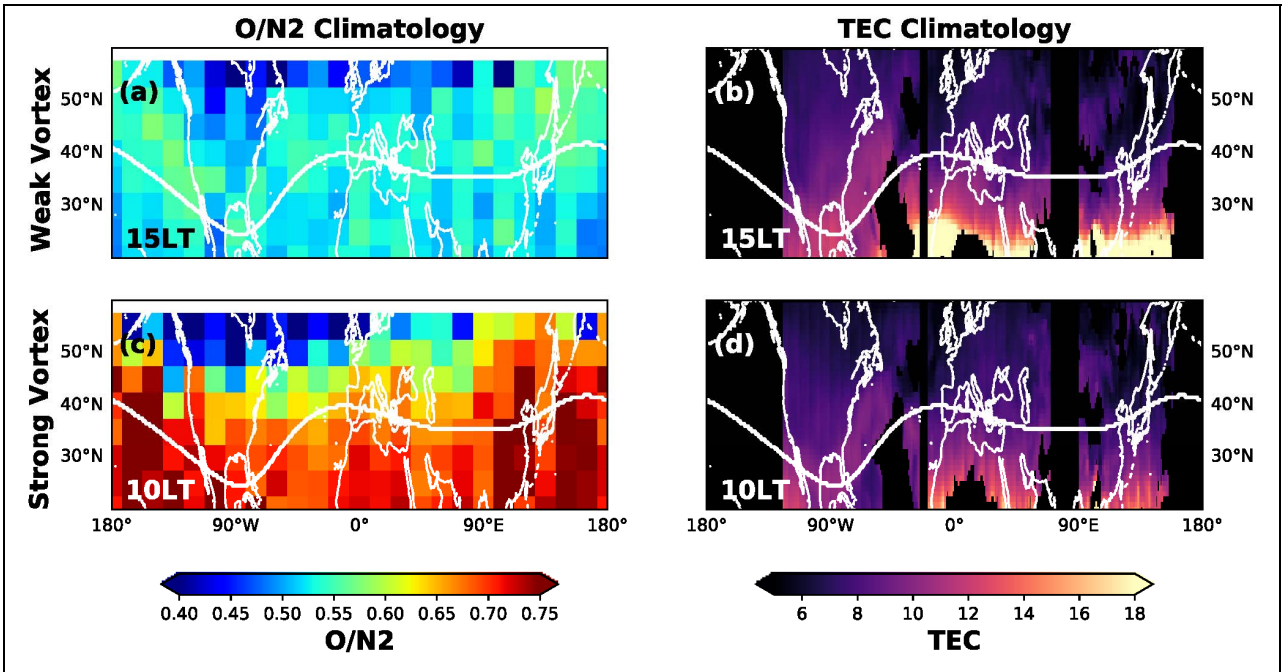

Figure 2. Climatologies of O/N_2 (left panels) and TEC (right panels) at 15 LT (top panels) and

10 LT (bottom panels). The thick white line is 35° magnetic latitude.

3.3 O/N_2 & TEC Anomalies

Figure 3 compares the events (colored symbols and colored lines) to the median thermospheric and ionospheric climatologies (black dashed lines) as a function of longitude at 35° magnetic latitude for the 3 days around the selected events. The gray shaded region represents the 25th to 75th percentiles of the climatologies. Panels (a) and (c) show O/N_2, while panels (b) and (d) show TEC. TEC data for the weak and strong events has been smoothed by taking the median of a bin that is +/- 5° longitude, +/-3° latitude, and +/- 30 minutes.

In general, during the weak vortex event (panel a) the O/N_2 is ~15% lower than the climatology and is outside the 25th percentile everywhere except the American sector. This is consistent with previous studies (e.g., Oberheide et al., 2020). Numerical simulations suggest that this is due to amplified tides and PWs during weak vortex events that affect the vertical transport of atomic oxygen in the lower thermosphere, leading to a reduction in O/N_2 that extends to midlatitudes (Jones et al., 2014a,b). There is little longitudinal variability in the suppressed O/N_2 in the weak vortex case.

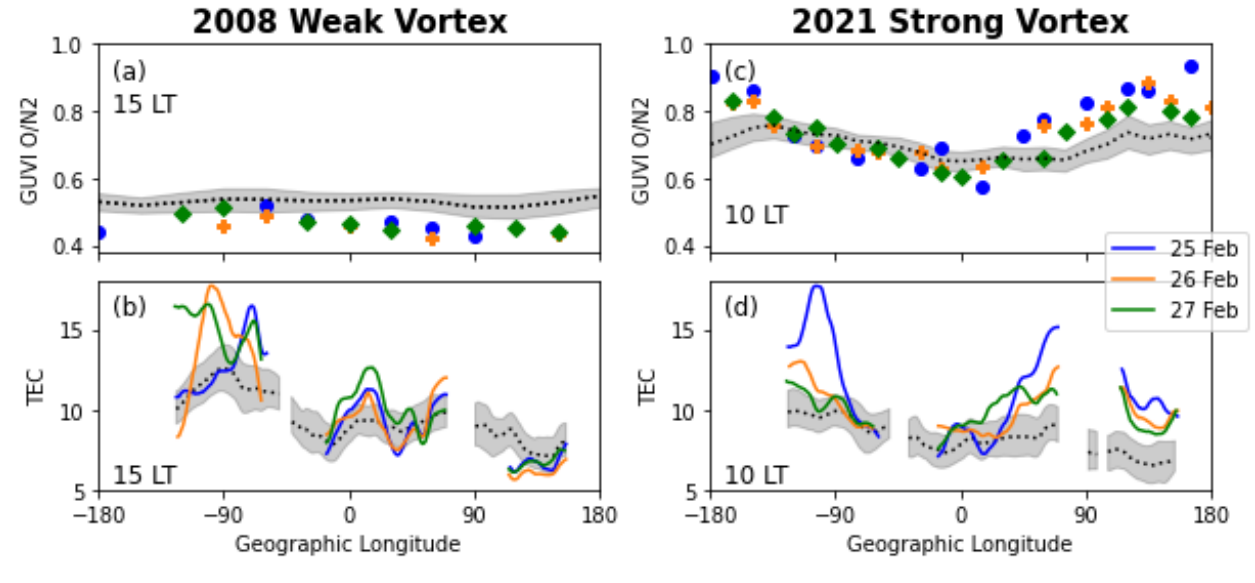

Figure 3. The O/N_2 climatology data (gray) and event data (in color) at 35° magnetic latitude for a weak vortex event (a) and strong vortex event (c) at constant local times. The TEC at the same magnetic latitude and local times are shown for the weak vortex event (b) and strong vortex event (d). The dotted lines are the median data from the quiet-time climatology, with shaded areas indicating the bounds of the 25th and 75th percentiles. Colored/line symbols are for individual days during the event.

During the strong vortex event (panel c) there is a striking longitudinal variability, a planetary "wave 1" pattern, with different longitude sectors exhibiting different behaviors. In the Asian sector, the O/N_2 is elevated by approximately 25%, while in the American sector O/N_2 is within the climatology. As we consider results at a fixed magnetic latitude, this variation is attributed to factors other than variations in magnetic latitude that are seen at a fixed geographic latitude. We largely attribute these O/N_2 changes to the changes in the tidal dissipation and MLT residual circulation during the weak and strong vortex events (Figure 1), which can alter the thermosphere O/N_2 (Oberheide et al., 2020; Pedatella, 2023). Specifically, when the vortex is weak, SW2 is strong and O/N_2 is reduced; the opposite is true when the vortex is strong. The large longitude asymmetry in O/N_2 in the strong vortex case may due to a longitude dependence of the meridional and vertical thermospheric winds advecting the neutral composition, and/or a longitudinal dependence in dissipating gravity waves. Complete understanding of these effects requires further observationally-based and modeling studies.

Figures 3 also shows the TEC at 35° magnetic latitude as a function of longitude for the weak vortex event (panel b) and the strong vortex event (panel d). It is evident that the ionospheric response to the strength of the vortex is complex. In the weak vortex case, the TEC is elevated over the climatology in the American sector, but suppressed compared to the climatology in the Asian sector. In the European sector, the TEC is close to the climatology. Significant longitudinal differences in mid-latitude ionospheric disturbances during weak polar vortex events were reported in numerous studies (Chen et al., 2016; Chernigovskaya et al., 2017; Oyama et al., 2015; Shpynev et al., 2015; Yue et al., 2010). The complex nature of ionospheric disturbances likely results from the superposition of several mechanisms and varying roles of thermospheric winds and geomagnetic fields. In the strong vortex case, ionospheric disturbances are less variable in longitude: the TEC is elevated in the Asian sector by up to 50%, near the climatology in the European and Eastern American sector, and again elevated over the Western American sector by 25-60%. Note, this longitude dependence would be obscured by zonal means. Clearly, strong vortex conditions have a significant impact on the ionospheric plasma content, though the detailed mechanisms generating the longitudinal variations require further study.

Figure 4 further explores the complex nature of the TEC variations during weak and strong polar vortices by showing the LT dependence at different longitudes, finding that some longitudes are dominated by composition driving the TEC. In the weak vortex case (top panels), there is an enhanced SW2 signature in TEC in the Western US sector (panel a) and possibly in the European sector (panel b), when TEC is increased during some LTs and suppressed 6 hours later. However, the TEC is depressed at 50° E (panel c) and 130° E (panel d) at most LTs. Lower TEC in these longitude sectors is consistent with decreased O/N_2 at these longitudes as shown in Figure 3a. Oyama et al. (2015) examined the relationship between composition and TEC in two different longitude sectors and also found a complex situation during the 2009 Arctic SSW. In the strong vortex case, over the Western US (panel e) there is enhanced TEC in the morning hours and TEC near climatology in the evening and nighttime hours. The European sector (panel f) is consistent with climatology. At 50° E longitude, there is elevated TEC in the morning hours followed by average conditions in the afternoon. Finally, the Asian sector (panel h) indicates elevated TEC throughout the day, suggesting that this behavior is not related to the enhanced SW2. The opposite TEC behavior in the Asian sector is particularly intriguing as it corresponds closely to the O/N_2 behavior seen in the Figure 3b.

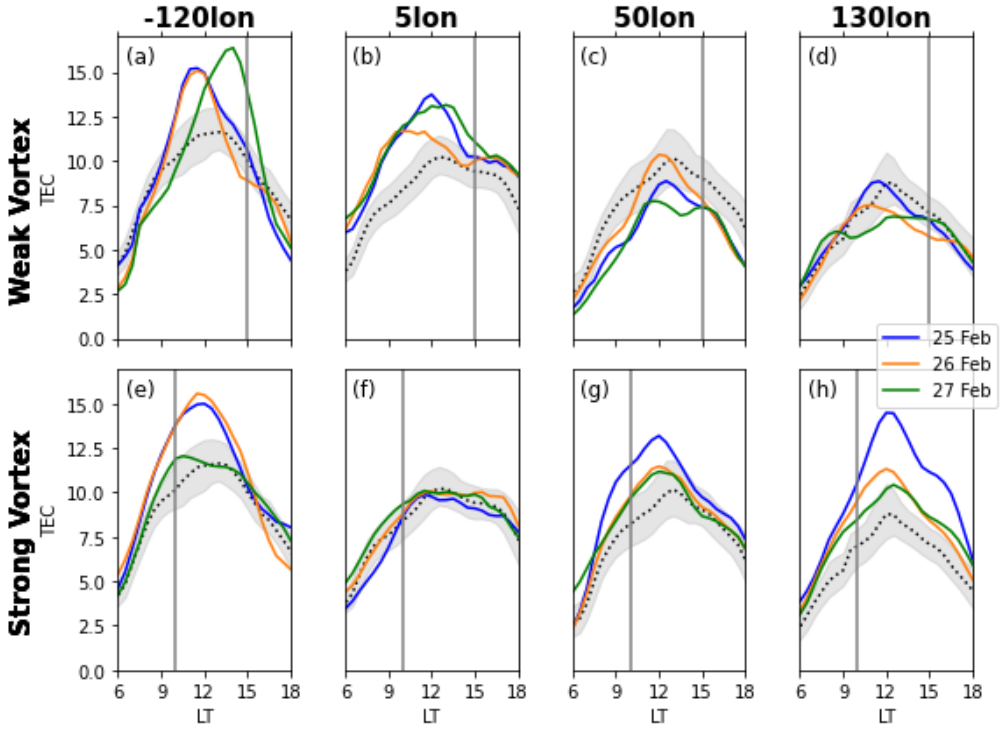

Figure 4. The LT behavior of the TEC climatology (black dashed line) and event data (solid lines) at 35° magnetic latitude for the weak vortex event (a-d) and strong vortex event (e-h) at different longitudes. The dotted lines are the median climatologies, with shaded areas indicating the bounds of the 25th and 75th percentiles. Colored lines are for individual days during the event. Vertical solid gray lines indicate the local times of the corresponding O/N_2 observations for the event.

Changes in TEC are driven by changes in at least three factors: (1) composition, (2) electric fields, and (3) neutral winds. The O/N_2 changes may indicate the extent to which chemistry is dominating the TEC changes during weak and strong vortex events. As O/N_2 increases, it increases the available source of O for production of O+ and an electron, increasing TEC. As O/N_2 decreases, the recombination rate increases, leading to lower plasma densities and lower TEC (Yamazaki & Richmond, 2013). Modified atmospheric tides may drive TEC enhancements or depletions (depending on phase of tides) through the E-region wind dynamo and modification of electric fields. Neutral winds have the ability to advect composition and drive vertical plasma drifts by blowing across geomagnetic field lines (Zhang et al., 2011), and both meridional and zonal components of neutral winds can significantly affect mid-latitude electron density. The relative importance of vertical drifts caused by thermospheric neutral winds vary depending on magnetic inclination and declination, and thus strongly vary with longitude. While electrodynamics play a lesser role in the midlatitudes, changes in thermospheric meridional winds act to change the F-region electron densities and peak height (Pedatella & Maute, 2015). A strong longitudinal dependence in meridional winds could, in turn, impart a longitudinal

dependence in TEC, in addition to any changes to composition, or electric field. Complete understanding of the mechanisms responsible for longitudinal variations in TEC during weak and strong vortex states is beyond the scope of this paper and is the subject of future work.

4. Conclusions

The stratospheric polar vortex exists in a continuum of states. At the extremes, a weak vortex or a strong vortex, there are noticeable impacts throughout the atmospheric column. Using two opposing case studies we examined the impact of the strength of the polar vortex on thermospheric composition and ionospheric plasma density at middle latitudes (35^{o} magnetic latitude). We conclude the following:

(1) The selected case studies of weak and strong vortex conditions have amplified and suppressed SW2 amplitudes, respectively. The resulting differences in tidal dissipation change the residual meridional circulation in the lower thermosphere and impact thermospheric composition.

(2) Both weak and strong polar vortex conditions are associated with significant longitudinal variations in thermospheric composition and ionospheric plasma content at midlatitudes.

(3) During the strong vortex case, O/N_2 is elevated by up to 25% compared to climatology over Asia. This increase in O/N_2 is observed for at least several days.

(4) During a strong vortex case, TEC is significantly enhanced over the climatology over Asia during all daytime hours. This indicates that increase in O/N_2 may be the main mechanism driving enhancement in the TEC at these longitudes.

(5) The ionospheric response at midlatitudes to weak and strong vortex events exhibits large longitudinal variability, which is thought to result from longitudinal differences in composition, thermospheric neutral winds, and electric fields.

(6) Disentangling the competing factors driving the longitudinal variations in TEC requires comprehensive observational and modeling studies that examine concurrently the thermospheric composition, thermospheric winds, electric fields, and TEC (or electron density profiles).

(7) The polar vortex is predictable up to two weeks in advance (e.g., Domeisen et al., 2020; Tripathi et al., 2009) and may provide valuable insights into forecasting thermospheric and ionospheric weather.

Acknowledgments

K.R.G., L.P.G., and V.L.H. acknowledge support from the NASA Heliophysics Guest Investigator grant 80NSSC19K0262 and NASA GOLD and ICON Guest Investigator grant 80NSSC22K0017. GNSS TEC data are provided at http://cedar.openmadrigal.org/ by MIT under support from NSF grant AGS-1952737. This material is based upon work supported by the National Center for Atmospheric Research, which is a major facility sponsored by the U.S. National Science Foundation under Cooperative Agreement 1852977. N. P. acknowledges support from NASA Grant 80NSSC18K1046 and 80NSSC20K1353.

Open Research

All of the data used in this paper are publicly available. TIMED GUVI O/N_2 data are available at http://guvitimed.jhuapl.edu/data_products. Microwave Limb Sounder v5.1 data are available from the NASA Goddard Space Flight Center for Earth Sciences Data and Information Services Center (DISC) at https://acdisc.gesdisc.eosdis.nasa.gov/data/Aura_MLS_Level2/. GPS TEC data

products and access through the Madrigal distributed data system are provided to the community (http://www.openmadrigal.org) by the Massachusetts Institute of Technology (MIT). WACCMX is part of the Community Earth System Model (CESM) and the source code is available at https://github.com/ESCOMP/CESM. The SD-WACCMX simulation output is available via https://doi.org/10.26024/5b58-nc53. We thank the NASA Global Modeling and Assimilation Office (GMAO) for making the MERRA-2 data available (via https://goldsmr5.gesdisc.eosdis.nasa.gov/data/MERRA2/M2I6NVANA.5.12.4/).

References

Baldwin, M. P., Ayarzagüena, B., Birner, T., Butchart, N., Butler, A. H., Charlton-Perez, A. J., et al. (2021). Sudden stratospheric warmings. Reviews of Geophysics, 59, e2020RG000708. https://doi.org/10.1029/2020RG000708

Charlton, A., and L. Polvani (2007), A new look at stratospheric sudden warmings. Part I: Climatology and modeling benchmarks, Journal of Climate, 20, 449–469, doi:10.1175/JCLI3996.1.

Chau, J. L., Fejer, B. G., & Goncharenko, L. P., (2009), Quiet variability of equatorial ExB drifts during a sudden stratospheric warming event, Geophysical Research Letters, 36, L05101. https://doi.org/10.1029/2008GL036785

Chau, J. L., Goncharenko, L. P., Fejer, B. G., & Liu, H.-L, (2012), Equatorial and low latitude ionospheric effects during sudden stratospheric warming events, Space Science Reviews, 168(1-4), 385–417. https://doi.org/10.1007/s11214-011-9797-5

Chau, J. L., P. Hoffmann, N. M. Pedatella, V. Matthias, and G. Stober (2015), Upper mesospheric lunar tides over middle and high latitudes during sudden stratospheric warming events, Journal of Geophysical Research - Space Physics, 120, 3084–3096, doi:10.1002/2015JA020998.

Chen, G., C. Wu, S. Zhang, B. Ning, X. Huang, D. Zhong, H. Qi, J. Wang, and L. Huang (2016), Midlatitude ionospheric responses to the 2013 SSW under high solar activity, Journal of Geophysical Research - Space Physics, 121, 790–803, doi:10.1002/2015JA021980.

Chernigovskaya, M.A., Shpynev, B. G., Ratovsky, K. G., Belinskaya, A.Yu., Stepanov, A.E., Bychkov, V.V., Grigorieva, S.A., Panchenko, V.A., Korenkova, N.A., Mielich, J. (2018), Ionospheric response to winter stratosphere/lower mesosphere jet stream in the Northern Hemisphere as derived from vertical radio sounding data, Journal of Atmospheric and Solar-Terrestrial Physics, 180, 126-136, https://doi.org/10.1016/j.jastp.2017.08.033.

Domeisen, D. I. V., Butler, A. H., Charlton-Perez, A. J., Ayarzagüena, B., Baldwin, M. P., Dunn-Sigouin, E., et al., (2020), The role of the stratosphere in subseasonal to seasonal prediction: 2. Predictability arising from stratosphere-troposphere coupling, Journal of Geophysical Research: Atmospheres, 125(2), e2019JD030923. https://doi.org/10.1029/2019JD030923

Fejer, B. G., M. E. Olson, J. L. Chau, C. Stolle, H. Lühr, L. P. Goncharenko, K. Yumoto, and T. Nagatsuma (2010), Lunar-dependent equatorial ionospheric electrodynamic effects during sudden stratospheric warmings, Journal of Geophysical Research - Space Physics,115, A00G03, doi:10.1029/2010JA015273.

Gan, Q., Qian, L., Pedatella, N. M., Wu, Y.-J., Correira, J., Wang, W., et al., (2023), GOLD synoptic observations of thermospheric annual and semiannual variations in composition during solar minimum years, Geophysical Research Letters, 50, e2022GL101215, https://doi.org/10.1029/2022GL101215

Gelaro, R., McCarty, W., Suárez, M. J., Todling, R., Molod, A., Takacs, L., et al., (2017), The modern-era retrospective analysis for research and applications, version 2 (MERRA-2), Journal of Climate, 30(14), 5419–5454, https://doi.org/10.1175/JCLI-D-16-0758.1

Goncharenko, L. P., A. J. Coster, R. A. Plumb, and D. I. V. Domeisen (2012), The potential role of stratospheric ozone in the stratosphere-ionosphere coupling during stratospheric warmings, Geophyiscal Research Letters, 39, L08101, doi:10.1029/2012GL051261.

Goncharenko, L. P., Harvey, V. L., Greer, K. R., Zhang, S.-R., Coster, A. J., (2020), Longitudinally dependent low-latitude ionospheric disturbances linked to the Antarctic sudden stratospheric warming of September 2019, Journal of Geophysical Research-Space Physics, 125, e2020JA028199. https://doi.org/10.1029/2020JA028199

Goncharenko, L. P., Harvey, V. L., Greer, K. R., Zhang, S.-R., Coster, A. J., & Paxton, L. J., (2021a), Impact of September 2019 Antarctic sudden stratospheric warming on mid-latitude ionosphere and thermosphere over North America and Europe, Geophysical Research Letters, 48, e2021GL094517. https://doi.org/10.1029/2021GL094517

Goncharenko, L., Harvey, V., Liu, H., & Pedatella, N, (2021b), Sudden stratospheric warming impacts on the ionosphere-thermosphere system—A review of recent progress, In C. Huang & G. Lu (Eds.), Space physics and aeronomy: Advances in ionospheric research: Current understanding and challenges (Vol. 3), Hoboken, NJ: Wiley.

Harvey, V.L., R.B. Pierce, T.D. Fairlie, & M.H. Hitchman, (2002), An object oriented climatology of stratospheric polar vortices and anticyclones, Journal of Geophysical Research - Atmosphere, https://doi.org/10.1029/2001JD001471

Harvey, V.L., C.E. Randall, L.P. Goncharenko, E. Becker, & J.A. France (2018), On the upward extension of the polar vortices into the mesosphere, Journal of Geophysical Research – Atmosphere, https://doi.org/10.1020/2018JD028815

Harvey, V.L., et al. (2022), Improving ionospheric predictability requires accurate simulation of the mesospheric polar vortex, Perspective, Frontiers Astronomy & Space Science - Space Physics, 9:1041426, https://doi.org/10.3389/fspas.2022.1041426

Jin, H., Y. Miyoshi, D. Pancheva, P. Mukhtarov, H. Fujiwara, and H. Shinagawa (2012), Response of migrating tides to the stratospheric sudden warming in 2009 and their effects on the ionosphere studied by a whole atmosphere-ionosphere model GAIA with COSMIC and TIMED/SABER observations, Journal of Geophysical Research, 117, A10323, doi:10.1029/2012JA017650.

Jones Jr., M., Forbes, J. M., Hagan, M. E., & Maute, A. (2014a), Impacts of vertically propagating tides on the mean state of the ionosphere-thermosphere system, Journal of Geophysical Research - Space Physics, 119, 2197–2213, https://doi.org/10.1002/2013JA019744

Jones Jr., M., Forbes, J. M., & Hagan, M. E. (2014b), Tidal-induced net transport effects on the oxygen distribution in the thermosphere, Geophysical Research Letters, 41, 5272–5279, https://doi.org/10.1002/2014GL060698

Kuroda, Y., and K. Kodera (1999), Role of planetary waves in the stratosphere-troposphere coupled variability in the Northern Hemisphere winter, Geophysical Research Letters, 26, 2375–2378.

Lawrence, Z. D., & Manney, G. L.(2018), Characterizing stratospheric polar vortex variability with computer vision techniques, Journal of Geophysical Research - Atmospheres, 123, 1510–1535, https://doi.org/10.1002/2017JD027556

Limpasuvan, V., Thompson, D. W. J., & Hartmann, D. L. (2004), The life cycle of the Northern Hemisphere sudden stratospheric warmings, Journal of Climate, 17(13), 2584–2596. https://doi.org/10.1175/1520-0442(2004)017

Limpasuvan, V., Y. J. Orsolini, A. Chandran, R. R. Garcia, and A. K. Smith (2016), On the composite response of the MLT to major sudden stratospheric warming events with elevated stratopause, Journal of Geophysical Research - Atmospheres., 121, 4518–4537, doi:10.1002/2015JD024401.

Liu, H.-L., Wang, W., Richmond, A. D., and Roble, R. G. (2010), Ionospheric variability due to planetary waves and tides for solar minimum conditions, Journal of Geophysical Research – Space Physics, 115, A00G01, doi:10.1029/2009JA015188

Liu, H.-L., Bardeen, C. G., Foster, B. T., Lauritzen, P., Liu, J., Lu, G., … Wang, W. (2018), Development and validation of the Whole Atmosphere Community Climate Model with thermosphere and ionosphere extension (WACCM-X 2.0), Journal of Advances in Modeling Earth Systems, 10, 381– 402, https://doi.org/10.1002/2017MS001232

Matsuno, T. (1971), A dynamical model of the stratospheric sudden warming, Journal of the Atmospheric Sciences, 28(8), 1479–1494, https://doi.org/10.1175/1520-0469

McDonald, S. E., F. Sassi, J. Tate, J. McCormack, D.D. Kuhl, D.P. Drob, C. Metzler, A.J. Mannucci, (2018), Impact of non-migrating tides on the low latitude ionosphere during a sudden stratospheric warming event in January 2010, Journal of Atmospheric and Solar-Terrestrial Physics, 171, 10.1016/j.jastp.2017.09.012.

Meier, R. R., et al. (2015), Remote Sensing of Earth's Limb by TIMED/GUVI: Retrieval of thermospheric composition and temperature, Earth and Space Science, 2, 1– 37, doi: 10.1002/2014EA000035.

Miyoshi, Y., H. Fujiwara, H. Jin, and H. Shinagawa (2015), Impacts of sudden stratospheric warming on general circulation of the thermosphere, Journal of Geophysical Reseach, 120, 10,897-10,912, doi:10.1002/ 2015JA021894.

Oberheide, J., Pedatella, N. M., Gan, Q., Kumari, K., Burns, A. G., & Eastes, R. (2020), Thermospheric composition O/N_2 response to an altered meridional mean circulation during Sudden Stratospheric Warmings observed by GOLD, Geophysical Research Letters, 47, e2019GL086313, https://doi.org/10.1029/2019GL086313

Oyama, K.-I., Jhou, J. T., Lin, J. T., Lin, C., Liu, H., and Yumoto, K. (2015), Ionospheric response to 2009 sudden stratospheric warming in the Northern Hemisphere, , Journal of Geophysical Reseach - Space Physics, 119, 10,260– 10,275, doi:10.1002/2014JA020014.

Pedatella, N. M., Liu, H.-L., Richmond, A. D., Maute, A., and Fang, T.-W. (2012), Simulations of solar and lunar tidal variability in the mesosphere and lower thermosphere during sudden stratosphere warmings and their influence on the low-latitude ionosphere, , Journal of Geophysical Reseach, 117, A08326, doi:10.1029/2012JA017858.

Pedatella, N. M., and Maute, A. (2015), Impact of the semidiurnal lunar tide on the midlatitude thermospheric wind and ionosphere during sudden stratosphere warmings, , Journal of Geophysical Reseach - Space Physics, 120, 10,740– 10,753, doi:10.1002/2015JA021986.

Pedatella, N. M., & Harvey, V. L. (2022), Impact of strong and weak stratospheric polar vortices on the mesosphere and lower thermosphere, Geophysical Research Letters, 49, e2022GL098877, https://doi.org/10.1029/2022GL098877

Pedatella, N. M., (2023), Influence of Stratosphere Polar Vortex Variability on the Mesosphere, Thermosphere, and Ionosphere, *Authorea*, doi: **10.22541/essoar.167979632.28660108/v1**

453 Qian, L., Burns, A. G., Wang, W., Solomon, S. C., and Zhang, Y. (2016), Longitudinal
454 variations of thermospheric composition at the solstices, , Journal of Geophysical
455 Reseach - Space Physics, 121, 6818– 6829, doi:10.1002/2016JA022898.
456 Randel, W. J. (1993), Global variations of zonal mean zonal ozone during stratospheric warming
457 events, J. Atmos. Sci., 50, 3308–3321.
458 Rideout, W., & Coster, A. (2006), Automated GPS processing for global total electron content
459 data, GPS Solutions, 10(3), 219–228, https://doi.org/10.1007/s10291-006-0029-5
460 Sathishkumar, S., and S. Sridharan (2013), Lunar and solar tidal variabilities in mesospheric
461 winds and EEJ strength over Tirunelveli (8.7 N, 77.8 E) during the 2009 major
462 stratospheric warming, , Journal of Geophysical Reseach - Space Physics, 118,
463 doi:10.1029/2012JA018236.
464 Scherhag, R. (1952), Die explosionsartigen Stratosphärenerwärmungen des Spätwinters 1951/52,
465 Berichte des deutschen Wetterdienstes in der US-Zone, 6(38), 51–63.
466 Schoeberl, M. R., Lait, L. R., Newman, P. A., and Rosenfield, J. E. (1992), The structure of the
467 polar vortex, Journal of Geophysical Reseach, 97(D8), 7859–7882,
468 https://doi.org/10.1029/91JD02168
469 Schwartz, M. J., Lambert, A., Manney, G. L., Read, W. G., Livesey, N. J., Froidevaux, L., et al.
470 (2008), Validation of the Aura Microwave Limb sounder temperature and geopotential
471 height measurements, Journal of Geophysical Research, 113(D15), D15S11,
472 https://doi.org/10.1029/2007JD008783
473 Shpynev, B.G., Kurkin, V.I., Ratovsky, K.G., Chernigovskaya, M.A., Belinskaya, A.Yu,
474 Grigorieva, S.A., Stepanov, A.E., Bychkov, V.V., Pancheva, D., Mukhtarov, P., (2015),
475 High-midlatitude ionosphere response to major stratospheric warming, Earth Planet,
476 Space 67 (18), http://dx.doi.org/10.1186/s40623-015-0187-1
477 Smith, A. K., Pedatella, N. M., Marsh, D. R., & Matsuo, T. (2017), On the dynamical control of
478 the mesosphere–lower thermosphere by the lower and middle atmosphere, Journal of the
479 Atmospheric Sciences, 74(3), 933–947, https://doi.org/10.1175/JAS-D-16-0226.1
480 Tripathi, O., Baldwin, M., Charlton-Perez, A., Charron, M., Cheung, J., Eckermann, S., Gerber,
481 E., Jackson, D., Kuroda, Y., Lang, A., McLay, J., Mizuta, R., Reynolds, C., Roff, G.,
482 Sigmond, M., Son, S.-W., and Stockdale, T., (2016), Examining the Predictability of the
483 Stratospheric Sudden Warming of January 2013 Using Multiple NWP Systems, Monthly
484 Weather Review 144, 5, https://doi.org/10.1175/MWR-D-15-0010.1
485 Vierinen, J., Coster, A. J., Rideout, W. C., Erickson, P. J., & Norberg, J. (2016), Statistical
486 framework for estimating GNSS bias, Atmospheric Measurement Techniques, 9(3),
487 1303-1312, https://doi.org/10.5194/amt-9-1303-2016
488 Waters, J. W., Froidevaux, L., Harwood, R. S., Jarnot, R. F., Pickett, H. M., Read, W. G., et al.
489 (2006), The Earth Observing System Microwave Limb Sounder (EOS MLS) on the Aura
490 satellite, IEEE Transactions on Geoscience and Remote Sensing, 44(5), 1075–1092,
491 doi:https://doi.org/10.1109/TGRS.2006.873771
492 Yamazaki, Y., & Richmond, A. D. (2013), A theory of ionospheric response to upward-
493 propagating tides: Electrodynamic effects and tidal mixing effects, Journal of
494 Geophysical Research: Space Physics, 118, 5891–5905,
495 https://doi.org/10.1002/jgra.50487
496 Yue, X., W. S. Schreiner, J. Lei, C. Rocken, D. C. Hunt, Y.-H. Kuo, and W. Wan (2010), Global
497 ionospheric response observed by COSMIC satellites during the January 2009

498 stratospheric sudden warming event, Journal of Geophysical Reseach, 115, A00G09,
499 doi:10.1029/2010JA015466.
500 Zhang, S.-R., Foster, J. C., Coster, A. J., and Erickson, P. J. (2011), East-West Coast differences
501 in total electron content over the continental US, Geophys. Res. Lett., 38, L19101,
502 doi:10.1029/2011GL049116.
503 Zhang, X., and J. M. Forbes (2014), Lunar tide in the thermosphere and weakening of the
504 northern polar vortex, Geophysical Research Letters, 41, 8201–8207,
505 doi:10.1002/2014GL062103.

Figure 1.

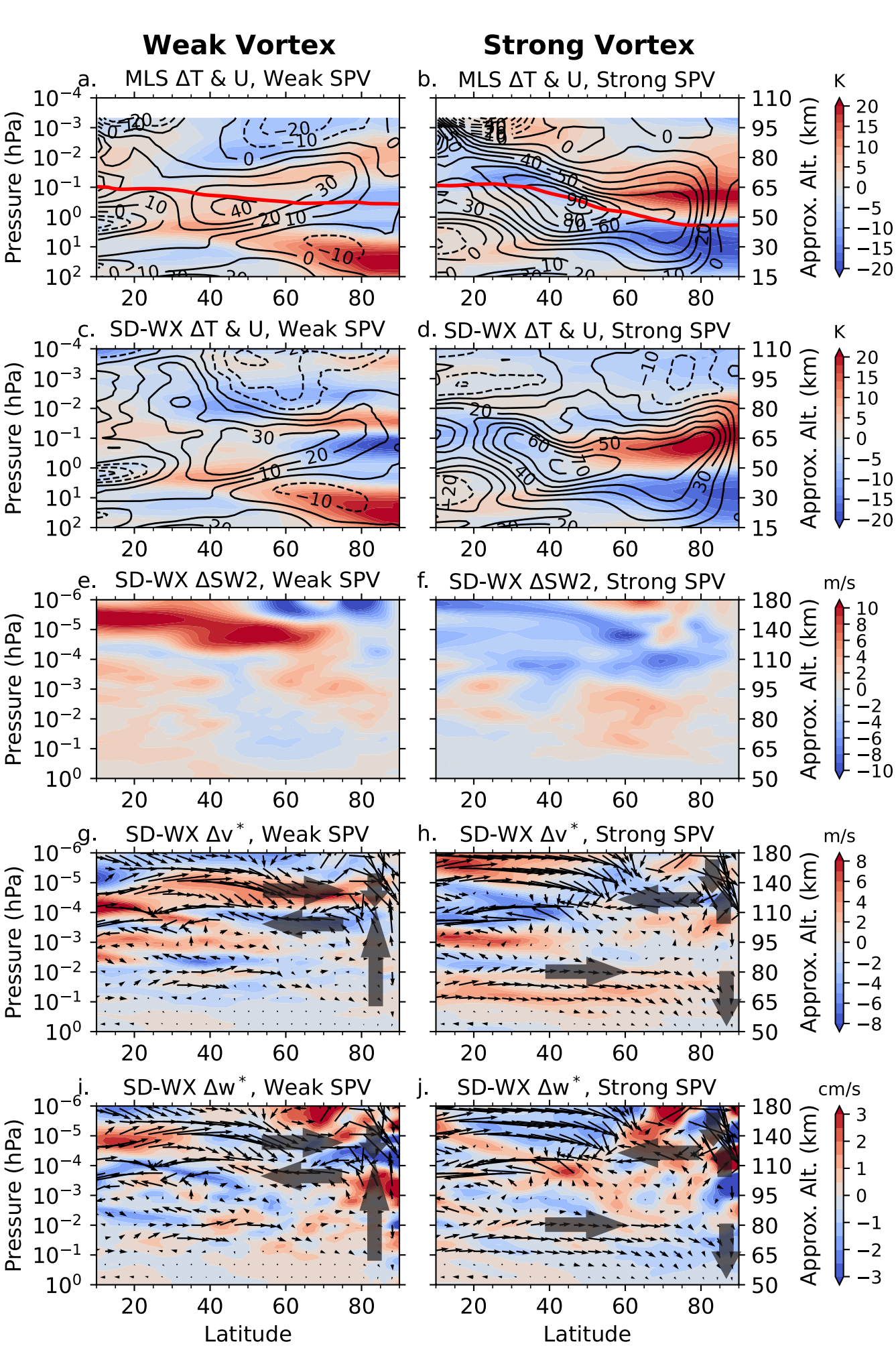
Weak Vortex
Strong Vortex
a. MLS ΔT & U, Weak SPV
b. MLS ΔT & U, Strong SPV
c. SD-WX ΔT & U, Weak SPV
d. SD-WX ΔT & U, Strong SPV
e. SD-WX ΔSW2, Weak SPV
f. SD-WX ΔSW2, Strong SPV
g. SD-WX Δv*, Weak SPV
h. SD-WX Δv*, Strong SPV
j. SD-WX Δw*, Weak SPV
j. SD-WX Δw*, Strong SPV
Pressure (hPa)
Approx. Alt. (km)
Latitude
K
m/s
cm/s

Figure 2.

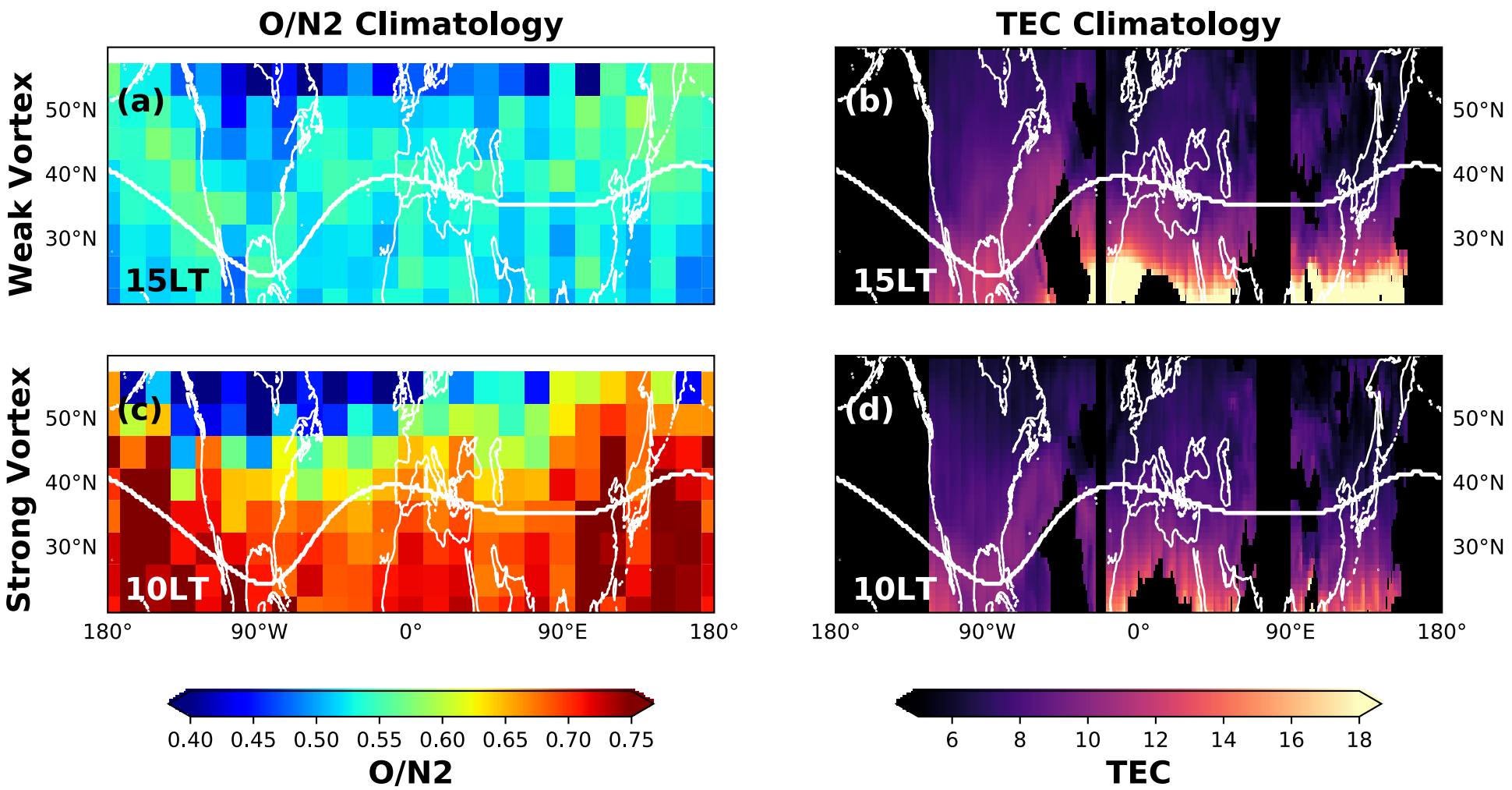
O/N2 Climatology
TEC Climatology
Weak Vortex
Strong Vortex
(a)
(b)
(c)
(d)
15LT
10LT
50°N
40°N
30°N
180°
90°W
0°
90°E
180°
0.40 0.45 0.50 0.55 0.60 0.65 0.70 0.75
O/N2
6 8 10 12 14 16 18
TEC

Figure 3.

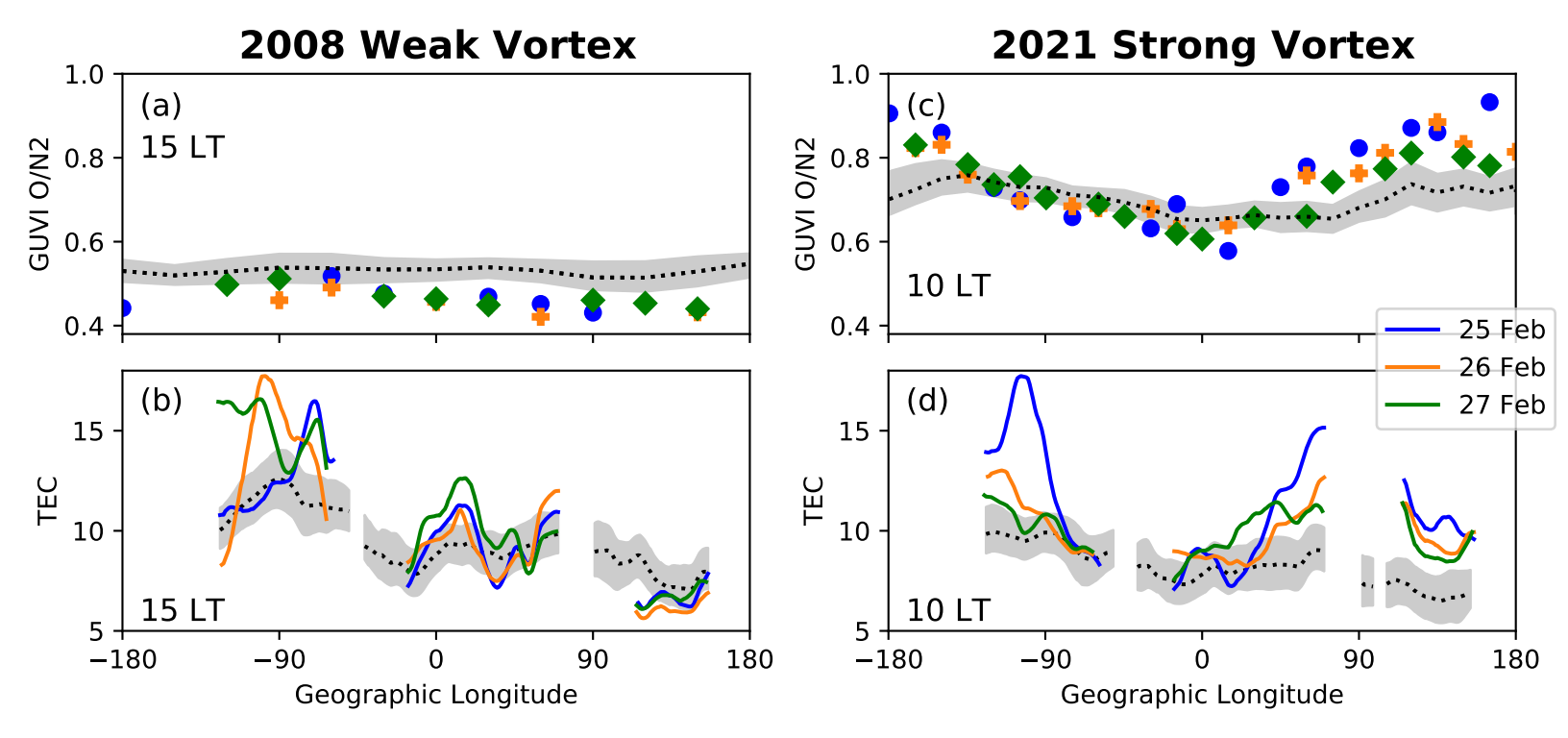
2008 Weak Vortex
2021 Strong Vortex
(a)
15 LT
(b)
15 LT
(c)
10 LT
(d)
10 LT
GUVI O/N2
TEC
Geographic Longitude
25 Feb
26 Feb
27 Feb
1.0
0.8
0.6
0.4
15
10
5
−180
−90
0
90
180

Figure 4.

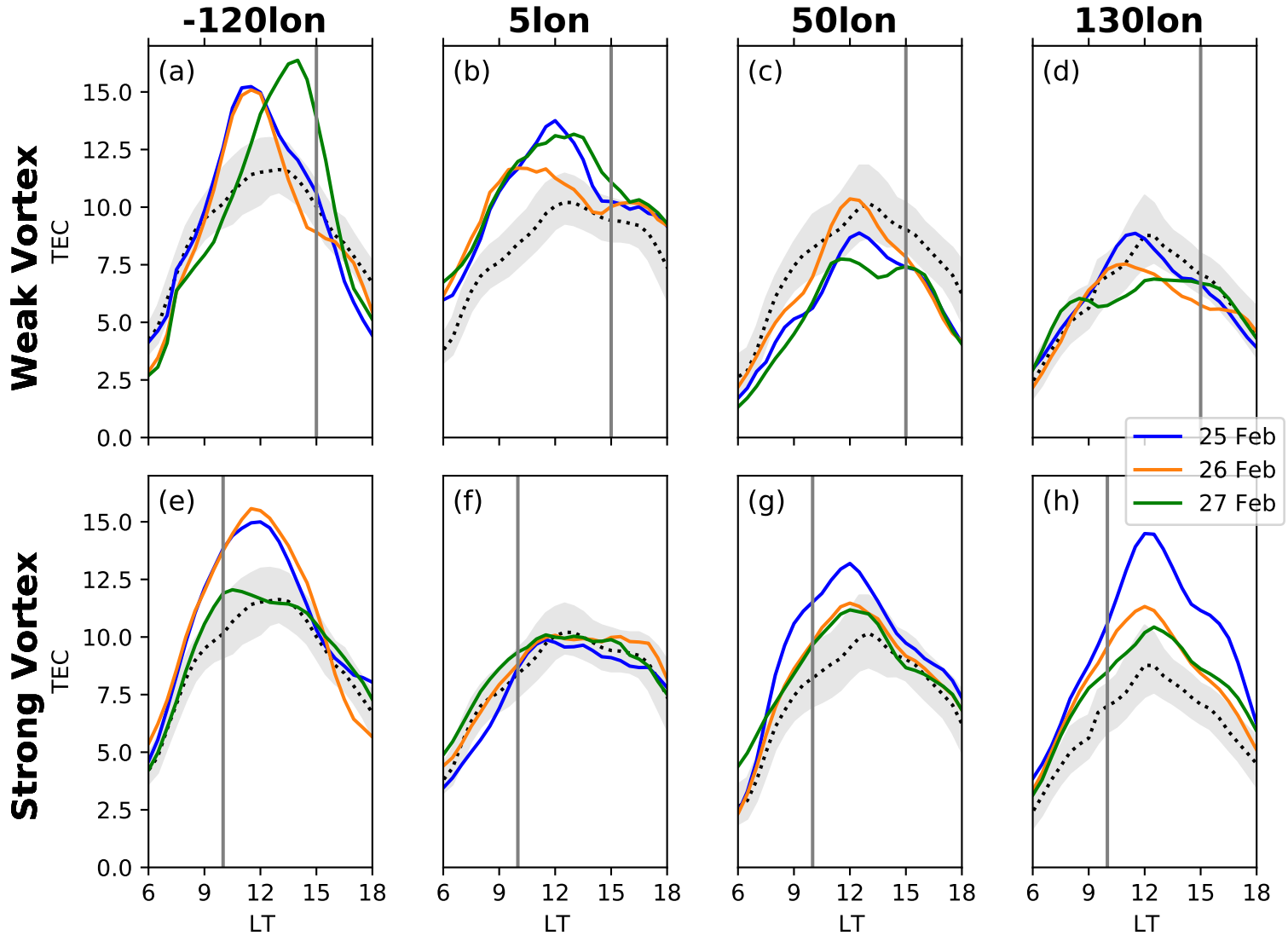
-120lon
5lon
50lon
130lon
Weak Vortex
Strong Vortex
TEC
LT
(a)
(b)
(c)
(d)
(e)
(f)
(g)
(h)
25 Feb
26 Feb
27 Feb
0.0
2.5
5.0
7.5
10.0
12.5
15.0
6
9
12
15
18